

New Na-Ion Solid Electrolytes $\text{Na}_{4-x}\text{Sn}_{1-x}\text{Sb}_x\text{S}_4$ ($0.02 \leq x \leq 0.33$) for All-Solid-State Na-Ion Batteries

Jongwook W. Heo, Abhik Banerjee, Kern Ho Park, Yoon Seok Jung,*
and Seung-Tae Hong*

Sulfide Na-ion solid electrolytes (SEs) are key to enable room-temperature operable all-solid-state Na-ion batteries that are attractive for large-scale energy storage applications. To date, few sulfide Na-ion SEs have been developed and most of the SEs developed contain P and suffer from poor chemical stability. Herein, discovery of a new structural class of tetragonal $\text{Na}_{4-x}\text{Sn}_{1-x}\text{Sb}_x\text{S}_4$ ($0.02 \leq x \leq 0.33$) with space group $I4_1/acd$ is described. The evolution of a new phase, distinctly different from Na_4SnS_4 or Na_3SbS_4 , allows fast ionic conduction in 3D pathways ($0.2\text{--}0.5 \text{ mS cm}^{-1}$ at 30°C). Moreover, their excellent air stability and reversible dissolution in water and precipitation are highlighted. Specifically, $\text{TiS}_2/\text{Na-Sn}$ all-solid-state Na-ion batteries using $\text{Na}_{3.75}\text{Sn}_{0.75}\text{Sb}_{0.25}\text{S}_4$ demonstrates high capacity ($201 \text{ mA h (g of TiS}_2\text{)}^{-1}$) with excellent reversibility.

Since the first demonstration of rechargeable Li batteries of TiS_2/Li in 1976,^[1] several important technical breakthroughs addressing safety issues, for example, the replacement of Li metal with carbonaceous materials as negative electrodes^[2] and the development of ceramic-coated separators,^[3,4] enabled widespread use of Li-ion batteries (LIBs) not only in portable electronic devices, but also in battery-driven electric vehicles. However, harsh engineering efforts to maximize energy density of LIBs, such as the use of ultrathin separators ($\leq 10 \mu\text{m}$) and raising the cutoff voltages, are deterred by serious safety concerns owing to the use of flammable organic liquid electrolytes.^[2,3,5,6] In this regard, use of solidifying electrolytes with inorganic materials is considered an ideal solution.^[7–11] Moreover, solid electrolytes (SEs) could enable the use of alternative electrode materials and/or stacking bipolar electrodes,

thus increasing the energy density of batteries.^[7–9,12]

Extensive developments of all-solid-state lithium-ion batteries to date relied on the discoveries of several state-of-the-art Li superionic conductors such as $\text{Li}_{9.54}\text{Si}_{1.74}\text{P}_{1.44}\text{S}_{11.7}\text{Cl}_{0.3}$ (25 mS cm^{-1})^[9] and $70\text{Li}_2\text{S}\cdot 30\text{P}_2\text{S}_5$ (17 mS cm^{-1}).^[13] Sulfide materials are more attractive than their counterparts owing to their superionic conductivities and softness, which allows surface contacts on active materials by simple cold-pressing process.^[7,14] The successes in developing sulfide Li-ion SEs led to the quest for new Na-ion SEs. Along with the inherent safety, all-solid-state Na-ion batteries (ASNBs) could leverage the advantage of Na-ion batteries


for cost-effectiveness and large-scale energy storage system solutions.^[15–17]

After the first report of the highly conductive sulfide Na-ion SE cubic Na_3PS_4 , which has a room-temperature conductivity of 0.2 or 0.46 mS cm^{-1} ,^[18,19] extensive progresses have been made, including the substitution of P with Si ($94\text{Na}_3\text{PS}_4\cdot 6\text{Na}_4\text{SiS}_4$, 0.74 mS cm^{-1})^[20] or As ($\text{Na}_3\text{P}_{0.62}\text{As}_{0.38}\text{S}_4$, 1.46 mS cm^{-1})^[21] and the substitution of S with Se (Na_3PSe_4 , 1.16 mS cm^{-1})^[22] or chlorine ($\text{Na}_{2.9375}\text{PS}_{3.9375}\text{Cl}_{0.0625}$, 1 mS cm^{-1}).^[23] Another type of SE, $\text{Na}_{10}\text{SnP}_2\text{S}_{12}$, with a conductivity of 0.4 mS cm^{-1} was also reported;^[24] however, all these materials contain P and suffer from poor air stability.^[16] Although the As-substitution for P in Li_3PS_4 enhanced the air stability,^[21] this improvement became less useful owing to the use of extremely toxic As. In contrast, our group reported the first phosphorus-free sulfide SE, tetragonal Na_3SbS_4 with a high ionic conductivity of 1.1 mS cm^{-1} and dry-air stability.^[16,25,26] Moreover, our group demonstrated that Na_3SbS_4 is solution processable using water or methanol,^[16] which is a breakthrough in achieving intimate ionic contacts by SE coatings on active materials and in fabricating sheet-type electrodes by an infiltration method.^[14,27,28] Further, more opportunities to find new sulfide Na-ion SEs exist, especially for phosphorus-free materials.

Herein, we report the discovery of a new structural class of Na-ion SEs. Substitution of Sn in an insulating Na_4SnS_4 with Sb results in the evolution of a new crystal structure with a chemical formula $\text{Na}_{4-x}\text{Sn}_{1-x}\text{Sb}_x\text{S}_4$ ($0.02 \leq x \leq 0.33$), distinct from Na_4SnS_4 or Na_3SbS_4 . The substitution drastically converts these materials into highly conductive Na-ion SEs (maximum conductivity of 0.51 mS cm^{-1} at 30°C), and the new phase

J. W. Heo, Prof. S.-T. Hong
Department of Energy Science and Engineering
DGIST (Daegu Gyeongbuk Institute of Science and Technology)
Daegu 42988, South Korea
E-mail: st.hong@dgist.ac.kr

Dr. A. Banerjee, Dr. K. H. Park, Prof. Y. S. Jung
School of Energy and Chemical Engineering
Department of Energy Engineering
UNIST (Ulsan National Institute of Science and Technology)
Ulsan 44919, South Korea
E-mail: ysjung@unist.ac.kr

 The ORCID identification number(s) for the author(s) of this article can be found under <https://doi.org/10.1002/aenm.201702716>.

DOI: 10.1002/aenm.201702716

shows excellent air stability and solution processability using water. Furthermore, good electrochemical performance of TiS₂/Na–Sn ASNBs using Na_{3.75}Sn_{0.75}Sb_{0.25}S₄ is demonstrated.

Na₄SnS₄ has a tetragonal crystal structure with $P\bar{4}2_1c$ symmetry consisting of two isolated SnS₄ tetrahedra per unit cell; one SnS₄ tetrahedron is located on the corner and the other at the center of the unit cell (Figure S1a, Supporting Information).^[29] Na₃SbS₄ has a similar structure, but fewer Na ions (Figure S1b, Supporting Information).^[16] Because of the structural similarity between Na₄SnS₄ and Na₃SbS₄, when a portion of Sn is replaced by Sb, a solid-solution phase with a nominal composition of Na_{4-x}Sn_{1-x}Sb_xS₄ is expected. However, an unknown phase appeared in the X-ray diffraction (XRD) patterns over a wide range of x values ($0.01 \leq x \leq 0.50$) (Figure 1a); the phase observed does not match any of the crystal structures in the database, implying that the phase has an unprecedented crystal structure. Even a 1% Sb substitution results in the formation of the unknown phase as a majority. The new phase is obtained in a high yield for the compositions in the range of $0.02 \leq x \leq 0.30$. At higher Sb content ($x = 0.40, 0.50$), a significant amount of Na₃SbS₄ also forms as a secondary phase. The new phase seems to be thermodynamically or kinetically stable under our synthetic conditions.

Variation of the ionic conductivity as a function of Sb substitution (x) in a series of Na_{4-x}Sn_{1-x}Sb_xS₄ is shown in Figure 1b (typical Nyquist plots for Ti/SE/Ti cells are shown in Figure S2, Supporting Information). For the samples prepared at 450 °C, the conductivity drastically increases as x increases from 0 (insulating, see Supporting Information for details) to 0.05 (0.060 mS cm⁻¹) and achieves the maximum value of 0.30 mS cm⁻¹ with an activation energy of 0.39 eV at $x = 0.40$. Although Na₃SbS₄ has a high ionic conductivity^[16] and Na₄SnS₄ is an insulator, such a drastic transition by a small substitution was not anticipated. The unusual change is in accord with the

change in the XRD patterns (Figure 1a), which strongly indicates that the new phase is responsible for the high conductivity. Interestingly, a slight decrease in conductivity in the range of $0.40 \leq x \leq 0.50$ is observed despite the growth of Na₃SbS₄. Given that the high conductivity of Na₃SbS₄ could stem from Na-ion vacancies,^[25,26] this abnormal behavior may imply that Na from the new phase Na_{4-x}Sn_{1-x}Sb_xS₄ grains moves to Na₃SbS₄ grains at the interfaces.^[30] Moreover, an additional synthetic trial indicates a possibility for a further optimization of the materials: Na_{3.75}Sn_{0.75}Sb_{0.25}S₄ prepared at 550 °C shows increased conductivity of 0.51 mS cm⁻¹.

The smooth fractured surfaces (Figure S3, Supporting Information) and the low porosity value of 11.5% for the cold-pressed Na_{3.75}Sn_{0.75}Sb_{0.25}S₄ pellet indicate good mechanical sinterability. From the cyclic voltammetry results scanned in the negative (0.0–3.0 V (vs. Na/Na⁺)) and positive (2.5–5.0 V (vs. Na/Na⁺)) voltage ranges (Figure S4, Supporting Information), the electrochemical stability window of Na_{3.75}Sn_{0.75}Sb_{0.25}S₄ is estimated to be ≈0.4–4.5 V (vs. Na/Na⁺). Importantly, the new materials showed excellent stability upon exposure to dry air for 24 h (Figure 1c; Figure S5, Supporting Information). Moreover, Na_{4-x}Sn_{1-x}Sb_xS₄ can be completely dissolved in water without the evolution of toxic H₂S gases and recrystallized by the evaporation of water and subsequent heat treatment at 450 °C under vacuum (Figures S6 and S7, Supporting Information), which shows a marginal decrease in ionic conductivities (Figure 1b). These unique characteristics of air-stability and solution-processability of Na_{4-x}Sn_{1-x}Sb_xS₄ are in stark contrast with the poor chemical stability of conventional phosphorus-based Na-ion SE materials.^[14,16]

Although the unknown phase appears in the XRD patterns over the entire range of x values, the sample with $x = 0.25$ was selected for structure determination because it seemed to have a less noticeable minor phase (3.4% of Na₃SbS₄ by weight,

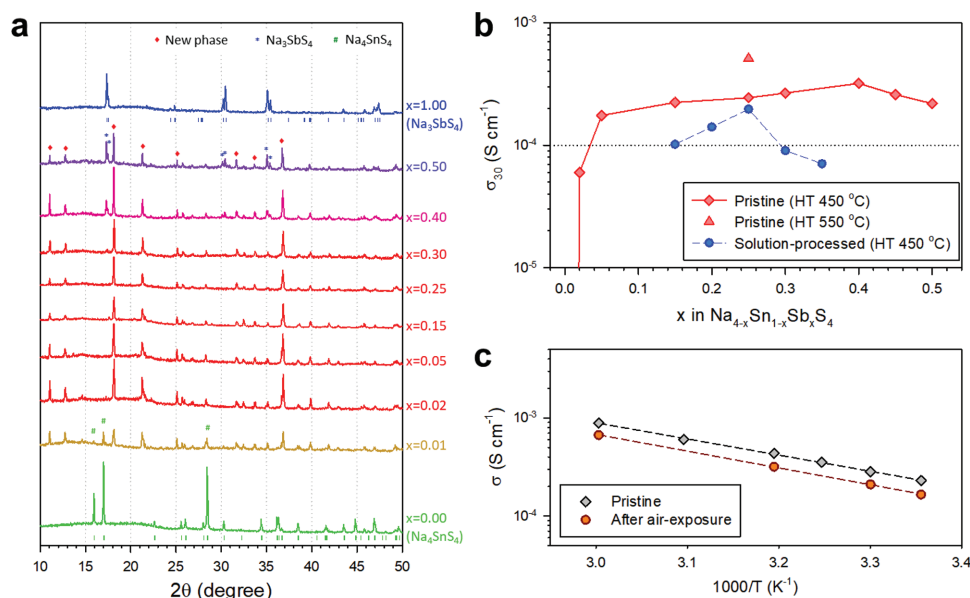


Figure 1. Characterization of Na_{4-x}Sn_{1-x}Sb_xS₄. a) XRD patterns for Na_{4-x}Sn_{1-x}Sb_xS₄. The Bragg positions for Na₃SbS₄^[16] and Na₄SnS₄ (JCPDS no. 65-1668) are shown. b) Ionic conductivities at 30 °C for pristine and aqueous-solution processed Na_{4-x}Sn_{1-x}Sb_xS₄. The heat-treatment temperatures for the samples are shown. c) Arrhenius plots of conductivities of Na_{3.75}Sn_{0.75}Sb_{0.25}S₄ before and after exposure to dry-air for 24 h.

estimated by the Rietveld refinement results). Combined elemental analysis using inductively coupled plasma optical emission spectroscopy (ICP-OES) (Table S1, Supporting Information) and Rietveld refinement results indicates that the chemical formula of the analyzed sample is $\text{Na}_{3.75}\text{Sn}_{0.75}\text{Sb}_{0.25}\text{S}_4$, which is consistent with the nominal composition. $\text{Na}_{3.75}\text{Sn}_{0.75}\text{Sb}_{0.25}\text{S}_4$ crystallizes in a tetragonal space group $I4_1/acd$ with $a = 13.8289(1) \text{ \AA}$, $c = 27.5179(4) \text{ \AA}$, $V = 5262.50(14) \text{ \AA}^3$, and $Z = 24$. The powder X-ray Rietveld refinement profile is shown in **Figure 2a**, the refinement results are summarized in Table S2 (Supporting Information), and the selected interatomic distances and angles are listed in Table S3 (Supporting Information). The crystal structure is presented with two different orientations for better visualization in **Figure 2b,c**. The positions of the

atoms in the unit cell were located from Fourier synthesis maps as shown in **Figure S8** (Supporting Information).

The unit cell contains one Sn site (16e), one Sb/Sn mixed site (8a), three S sites (all 32g), and five Na sites (16c, 16d, 16e, 16f, and 32g, respectively). All Na sites have a small deficiency with an average occupancy of 93.7%. These crystallographic results (Table S2, Supporting Information) provide insights into the compositions that can be achieved as a single phase in the $\text{Na}_{4-x}\text{Sn}_{1-x}\text{Sb}_x\text{S}_4$ series, where the Sb/Sn ratio in the 8a site is variable. When the 8a site is fully occupied by Sb, it becomes an ideal stoichiometric compound with the chemical formula, $\text{Na}_{3.667}\text{Sn}_{0.667}\text{Sb}_{0.333}\text{S}_4$, or $\text{Na}_{11}\text{Sn}_2\text{SbS}_{12}$. The upper limit of Sb substitution is 33.3%, which is in good agreement with the observed XRD data (**Figure 1a**), where higher compositions

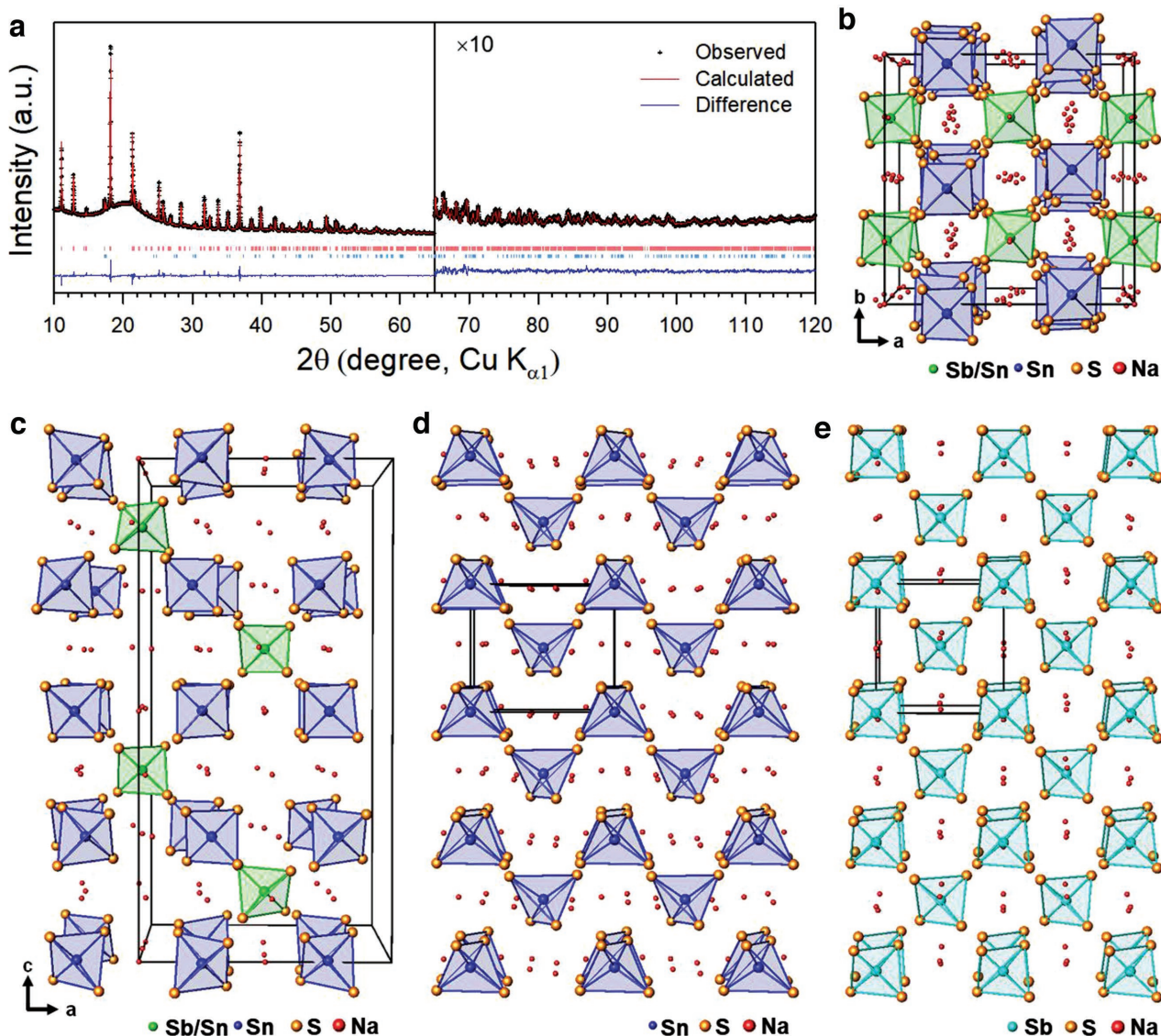


Figure 2. Structural analysis results of $\text{Na}_{3.75}\text{Sn}_{0.75}\text{Sb}_{0.25}\text{S}_4$ compared with Na_4SnS_4 and Na_3SbS_4 . a) Observed and calculated powder X-ray Rietveld refinement profiles for $\text{Na}_{3.75}\text{Sn}_{0.75}\text{Sb}_{0.25}\text{S}_4$ recorded at 25°C . Bragg positions for $\text{Na}_{3.75}\text{Sn}_{0.75}\text{Sb}_{0.25}\text{S}_4$ (pale red) and Na_3SbS_4 (3.4% by weight, pale blue), respectively. Crystal structure of $\text{Na}_{3.75}\text{Sn}_{0.75}\text{Sb}_{0.25}\text{S}_4$, b) (001), and c) (010) view. To clearly show 1:1 ordering of SnS_4 (purple) and SbS_4 (green) tetrahedra, only front half of the unit cell is presented in c) ($\text{Sb}' \equiv \text{Sb/Sn}$ mixed site). Crystal structures of d) Na_4SnS_4 and e) Na_3SbS_4 in (010) view. The unit cells are outlined in the views.

with $x = 0.40$ and 0.50 resulted in the formation of a significant amount of Na_3SbS_4 as a secondary phase. The lower limit of Sb substitution appears to be approximately 2%. X-ray Rietveld refinement for the samples with $x = 0.05$ (Figure S9, Supporting Information) and $x = 0.50$ (Figure S10, Supporting Information) also shows that both are isostructural with $x = 0.25$, except for the Sb/Sn ratio of the 8a site and the number of Na ions. The chemical compositions analyzed by ICP-OES (Table S1, Supporting Information) and Rietveld refinement shows that each of samples has a secondary impurity phase—1.9% of Na_2S and 24% of Na_3SbS_4 by weight, respectively, and the chemical formulas are $\text{Na}_{3.95}\text{Sn}_{0.95}\text{Sb}_{0.05}\text{S}_4$ (Table S4, Supporting Information) and $\text{Na}_{3.67}\text{Sn}_{0.67}\text{Sb}_{0.33}\text{S}_4$ (Table S5, Supporting Information), respectively, verifying the upper limit of Sb substitution ($x = 1/3$).

The new structure of $\text{Na}_{3.75}\text{Sn}_{0.75}\text{Sb}_{0.25}\text{S}_4$ can be characterized by the isolated MS_4 ($M = \text{Sn}, \text{Sb}$) tetrahedra that are interconnected by Na ions, which is also a similar characteristic of Na_4SnS_4 (or Na_3SbS_4). The apparent difference is that Na_4SnS_4 (or Na_3SbS_4) has only one type of SnS_4 (or SbS_4) tetrahedron, but the new structure has two crystallographically distinct types of sites, namely a Sn-only site (16e) and an Sb-rich (Sb/Sn mixed) site (8a). Figure 2b,c shows clearly that SnS_4 tetrahedra and Sb-rich tetrahedra (hereafter, $\text{Sb}'\text{S}_4$) are ordered in such a way that SnS_4 tetrahedra form a pseudo-cubic sublattice (with a length of $\approx 6.9 \text{ \AA}$), and the center of the subcell is filled with $\text{Sb}'\text{S}_4$. However, only half of the centers are filled with $\text{Sb}'\text{S}_4$, leaving the other half vacant (Figure 2c; Figure S11, Supporting Information), and $\text{Sb}'\text{S}_4$ and the vacancy form a 1:1 ordering in three dimensions. The new structure can be regarded as a $2 \times 2 \times 4$ superstructure of Na_4SnS_4 (or Na_3SbS_4)—doubling in a and b -axes and quadrupling in the c -axis (Figure 2b–e). The local environments of SnS_4 and $\text{Sb}'\text{S}_4$ are indistinguishable in terms of tetrahedral symmetry, but clearly distinguished by interatomic distances between metal and sulfur atoms— $d(\text{Sn}-\text{S})$ is 2.420 \AA that is longer than 2.312 \AA for $d(\text{Sb}'-\text{S})$.

Presuming ion diffusion takes place along the Na networks, the connectivity of Na atoms should be an important parameter for the conductivity. Interestingly, despite the complexity of the structure, the interatomic distances between neighboring Na atoms are evenly distributed within a narrow range of $3.42\text{--}3.53 \text{ \AA}$. The Na chains exist in all three directions parallel to the crystal axes, enabling 3D diffusion in this structure. It is also noted that the Na pathways are not straight, but zigzagged or sinusoidal (Figure S12, Supporting Information).

The empirical expression for bond valence has been widely adopted to estimate valences in inorganic solids, and was used in this work to confirm the validity of the newly determined crystal structure (see Experimental Section in the Supporting Information for detail). Recently, it has been demonstrated that the 3D bond-valence sum mappings (BVSM)^[31] can also be used for probing the ion conduction pathways of the inorganic materials. Indeed, the BVSM calculation shows the possible Na-ion diffusion pathways. Figure 3 and Figure S13 (Supporting Information) represent the isosurfaces for Na ions, clearly demonstrating a 3D network of the Na-ion diffusion pathways along the a (or b) and c -axes, confirming the high ionic conductivity of $\text{Na}_{4-x}\text{Sn}_{1-x}\text{Sb}_x\text{S}_4$. Nonetheless, it should be noted that the diffusion channel shown by the BVSM is a necessary condition for fast diffusion, but it does not explain

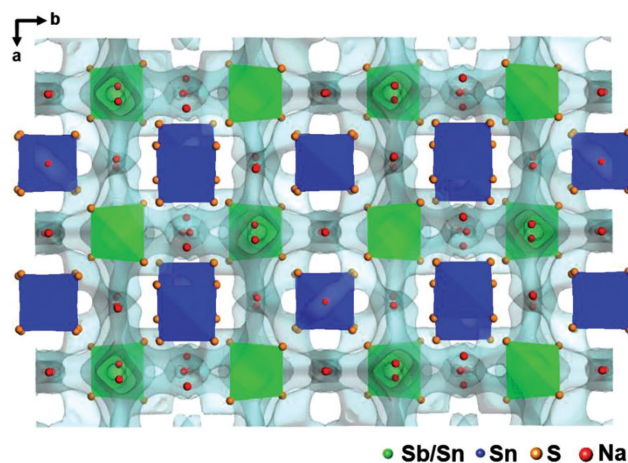


Figure 3. 3D bond valence difference map isosurfaces (sky-blue color) for $\text{Na}_{3.75}\text{Sn}_{0.75}\text{Sb}_{0.25}\text{S}_4$ with isosurfaces of $|0.1|$ v.u. for Na ions. Na atoms are shown as red balls. SnS_4 and $\text{Sb}'\text{S}_4$ are shown as blue and green tetrahedra, respectively ($\text{Sb}' \equiv \text{Sb/Sn}$ mixed site).

why the new structure works better. A further comprehensive analysis, including a computational method, should be performed to better understand why a superstructure is preferentially stabilized, not forming a solid solution, and the in-depth origin of fast ionic conduction in this new structure.^[10,32]

Finally, $\text{TiS}_2/\text{Na-Sn}$ ASNBs fabricated using $\text{Na}_{3.75}\text{Sn}_{0.75}\text{Sb}_{0.25}\text{S}_4$ were cycled between 1.0 and 2.5 V at $30 \text{ }^\circ\text{C}$. Figure 4a shows the first two-cycle discharge-charge voltage

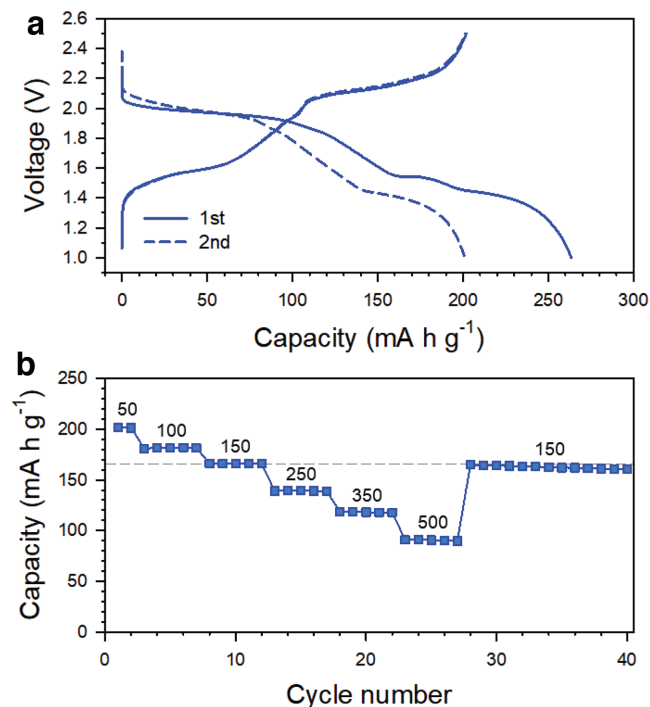


Figure 4. Electrochemical performance of $\text{TiS}_2/\text{Na-Sn}$ all-solid-state cell using $\text{Na}_{3.75}\text{Sn}_{0.75}\text{Sb}_{0.25}\text{S}_4$ at $30 \text{ }^\circ\text{C}$. a) First two-cycle charge-discharge voltage profiles at $50 \mu\text{A cm}^{-2}$ (0.06C). b) Charge capacity as a function of cycle number, varied by different current densities. The numbers are the current densities in $\mu\text{A cm}^{-2}$.

profiles at $50 \mu\text{A cm}^{-2}$. TiS_2 with $\text{Na}_{3.75}\text{Sn}_{0.75}\text{Sb}_{0.25}\text{S}_4$ exhibits a high reversible capacity of $201 \text{ mA h (g of TiS}_2\text{)}^{-1}$, which is much higher than those in previous reports on ASNBs^[21,23] and comparable to those in previous reports on Na-ion batteries using liquid electrolytes.^[15,33] The charge capacity as a function of cycle number, varied by different C-rates, are also shown in Figure 4b (the corresponding voltage profiles are shown in Figure S14, Supporting Information). TiS_2 in Na-ion batteries with liquid electrolytes suffer from poor reversibility.^[33] Notably, TiS_2 with the SE $\text{Na}_{3.75}\text{Sn}_{0.75}\text{Sb}_{0.25}\text{S}_4$ retained 99.4% of its capacity at the 8th cycle after 20 cycles, highlighting the excellent compatibility between TiS_2 and $\text{Na}_{3.75}\text{Sn}_{0.75}\text{Sb}_{0.25}\text{S}_4$. The rate capability, however, is not excellent compared to that of the state-of-the-art, all-solid-state LIBs in previous reports,^[9,14] which calls for a need to enhance the ionic conductivity of SEs and engineer the interfaces.

In summary, a new structural class of highly conductive Na-ion SEs $\text{Na}_{4-x}\text{Sn}_{1-x}\text{Sb}_x\text{S}_4$ ($0.02 \leq x \leq 0.33$) was discovered in the course of systematic investigation of materials with a range of nominal compositions of $0.0 \leq x \leq 0.50$. The new structure in the tetragonal space group $I4_1/acd$ was fully identified by ab initio X-ray structural analysis, consisting of Sn-only and Sb/Sn mixed sites in a tetrahedral coordination. The BVSM revealed the 3D Na-ion diffusion pathways in the new phase, which allowed the high ionic conductivities ($0.2\text{--}0.5 \text{ mS cm}^{-1}$ at 30°C). Moreover, the new $\text{Na}_{4-x}\text{Sn}_{1-x}\text{Sb}_x\text{S}_4$ materials showed excellent dry-air stability, no H_2S evolution in contact with water, and reversible precipitation from the homogeneously dissolved aqueous solution, highlighting their potential practical applications. Finally, the high capacity and stable cycling performance of $\text{TiS}_2/\text{Na-Sn ASNBs}$ using $\text{Na}_{3.75}\text{Sn}_{0.75}\text{Sb}_{0.25}\text{S}_4$ were successfully demonstrated. As gathered from the research in Na_3PS_4 -based materials, the conductivity of $\text{Na}_{4-x}\text{Sn}_{1-x}\text{Sb}_x\text{S}_4$ could be further enhanced by the exploration of iso- and/or aliovalent substitution, and by the optimization of synthetic conditions, which are now underway. Our discovery of this new Na-ion SEs with a complete structural solution will ignite interests in theoretical study on the ionic conduction mechanism relevant to structure, designing new superionic conductors, and contributing to progress in practical all-solid-state technologies.

Experimental Section

Preparation of Materials: $\text{Na}_{4-x}\text{Sn}_{1-x}\text{Sb}_x\text{S}_4$ powders were prepared by heat-treatment of stoichiometric mixture of Na_2S (Sigma Aldrich), SnS_2 (Kojundo Chemical Laboratory, 99.9%), Sb_2S_3 (99.5%, Sigma Aldrich), and elemental sulfur (99.5%, Alfa Aesar) at 450°C or 550°C for 12 h in a fused-silica ampoule sealed under vacuum. The Na_3PS_4 powders were prepared by mechanochemical milling of stoichiometric mixture of Na_2S and P_2S_5 (99%, Sigma Aldrich) for 10 h, followed by heat-treatment at 270°C for 1 h in a sealed glass ampoule. For the solution-process of $\text{Na}_{4-x}\text{Sn}_{1-x}\text{Sb}_x\text{S}_4$, the as-prepared $\text{Na}_{4-x}\text{Sn}_{1-x}\text{Sb}_x\text{S}_4$ powders were fully dissolved into deionized water under dry Ar. After the powders were dried under vacuum at room temperature, further heat-treatment was carried out in a sealed glass ampoule at 450°C .

Materials Characterization: The chemical composition of $\text{Na}_{4-x}\text{Sn}_{1-x}\text{Sb}_x\text{S}_4$ was measured by ICP-OES using the 720-ES (Varian Corp.). For the test of dry-air stability, 200 mg of SE powders was kept under continuous flow of dry air (a mixture of O_2 and N_2 with 21/79 vol ratio) for 24 h.

Electrochemical Characterization: After the $\text{Na}_{4-x}\text{Sn}_{1-x}\text{Sb}_x\text{S}_4$ pellets were prepared by cold-pressing at 370 MPa, the ionic conductivity was measured by an AC impedance method using an Iviumstat (IVIUM Technologies Corp.) with symmetric Na-ion blocking Ti/SE/Ti cells. All-solid-state Na-ion cells were fabricated as follows: Composite electrodes were prepared from the $\text{TiS}_2/\text{Na}_{3.75}\text{Sn}_{0.75}\text{Sb}_{0.25}\text{S}_4$ mixture with 1:1 weight ratio. Na_3Sn prepared by mixing of Na metal (Sigma Aldrich) with Sn metal powders (Sigma Aldrich) served as the counter electrode, exhibiting an operating voltage of $\approx 0 \text{ V (vs. Na/Na}^+)$. A $\text{Na}_{3.75}\text{Sn}_{0.75}\text{Sb}_{0.25}\text{S}_4/\text{Na}_3\text{PS}_4$ bilayer pellet (150, 20 mg, respectively) prepared by cold-pressing under 370 MPa was used as the SE layer. 10 mg of the as-prepared mixture electrodes was spread on the $\text{Na}_{3.75}\text{Sn}_{0.75}\text{Sb}_{0.25}\text{S}_4$ side of SE bilayer, followed by pressing at 370 MPa. Then, 50 mg of the as-prepared Na_3Sn was attached on the other side (Na_3PS_4) of SE bilayer by pressing at 370 MPa. All the procedures were performed in a polyaryletheretherketone mold (diameter = 13 mm) with two Ti metal rods as current collectors. All processes for fabricating the all-solid-state cells were performed in an Ar-filled dry box. Galvanostatic charge–discharge measurements were performed at 30°C between 1.0 and 2.5 V.

Supporting Information

Supporting Information is available from the Wiley Online Library or from the author.

Acknowledgements

J.W.H., A.B., and K.H.P. contributed equally to this work. This work was supported by Basic Science Research Program (No. NRF-2017M1A2A2044501) and by Leading Foreign Research Institute Recruitment Program (No. NRF-2017K1A4A3015437) through the National Research Foundation of Korea (NRF) funded by the Ministry of Science, ICT & Future Planning, and by the Materials and Components Technology Development Program of MOTIE/KEIT (10076731).

Conflict of Interest

The authors declare no conflict of interest.

Keywords

crystal structures, ionic conductivities, solid electrolytes, solid-state batteries, sulfides

Received: September 28, 2017

Revised: October 31, 2017

Published online: January 15, 2018

- [1] M. S. Whittingham, *Science* **1976**, 192, 1126.
- [2] J. B. Goodenough, Y. Kim, *Chem. Mater.* **2010**, 22, 587.
- [3] P. Arora, Z. Zhang, *Chem. Rev.* **2004**, 104, 4419.
- [4] Y. S. Jung, A. S. Cavanagh, L. Gedvilas, N. E. Widjonarko, I. D. Scott, S. H. Lee, G. H. Kim, S. M. George, A. C. Dillon, *Adv. Energy Mater.* **2012**, 2, 1022.
- [5] H. Wu, D. Zhuo, D. S. Kong, Y. Cui, *Nat. Commun.* **2014**, 5, 5193.
- [6] K. Xu, *Chem. Rev.* **2014**, 114, 11503.
- [7] Y. S. Jung, D. Y. Oh, Y. J. Nam, K. H. Park, *Israel J. Chem.* **2015**, 55, 472.
- [8] J. Janek, W. G. Zeier, *Nat. Energy* **2016**, 1, 16141.

- [9] Y. Kato, S. Hori, T. Saito, K. Suzuki, M. Hirayama, A. Mitsui, M. Yonemura, H. Iba, R. Kanno, *Nat. Energy* **2016**, *1*, 16030.
- [10] Y. Wang, W. D. Richards, S. P. Ong, L. J. Miara, J. C. Kim, Y. Mo, G. Ceder, *Nat. Mater.* **2015**, *14*, 1026.
- [11] A. Manthiram, X. Yu, S. Wang, *Nat. Rev. Mater.* **2017**, *2*, 16103.
- [12] X. Han, Y. Gong, K. K. Fu, X. He, G. T. Hitz, J. Dai, A. Pearse, B. Liu, H. Wang, G. Rubloff, Y. Mo, V. Thangadurai, E. D. Wachsman, L. Hu, *Nat. Mater.* **2017**, *16*, 572.
- [13] Y. Seino, T. Ota, K. Takada, A. Hayashi, M. Tatsumisago, *Energy Environ. Sci.* **2014**, *7*, 627.
- [14] K. H. Park, D. Y. Oh, Y. E. Choi, Y. J. Nam, L. Han, J.-Y. Kim, H. Xin, F. Lin, S. M. Oh, Y. S. Jung, *Adv. Mater.* **2016**, *28*, 1874.
- [15] N. Yabuuchi, K. Kubota, M. Dahbi, S. Komaba, *Chem. Rev.* **2014**, *114*, 11636.
- [16] A. Banerjee, K. H. Park, J. W. Heo, Y. J. Nam, C. K. Moon, S. M. Oh, S.-T. Hong, Y. S. Jung, *Angew. Chem., Int. Ed.* **2016**, *55*, 9634.
- [17] Y. Yan, R.-S. Kühnel, A. Remhof, L. Duchêne, E. C. Reyes, D. Rentsch, Z. Łodziana, C. Battaglia, *Adv. Energy Mater.* **2017**, *7*, 1700294.
- [18] A. Hayashi, K. Noi, A. Sakuda, M. Tatsumisago, *Nat. Commun.* **2012**, *3*, 856.
- [19] A. Hayashi, K. Noi, N. Tanibata, M. Nagao, M. Tatsumisago, *J. Power Sources* **2014**, *258*, 420.
- [20] N. Tanibata, K. Noi, A. Hayashi, M. Tatsumisago, *RSC Adv.* **2014**, *4*, 17120.
- [21] Z. Yu, S.-L. Shang, J.-H. Seo, D. Wang, X. Luo, Q. Huang, S. Chen, J. Lu, X. Li, Z.-K. Liu, D. Wang, *Adv. Mater.* **2017**, *29*, 1605561.
- [22] L. Zhang, K. Yang, J. Mi, L. Lu, L. Zhao, L. Wang, Y. Li, H. Zeng, *Adv. Energy Mater.* **2015**, *5*, 1501294.
- [23] I. H. Chu, C. S. Kompella, H. Nguyen, Z. Y. Zhu, S. Hy, Z. Deng, Y. S. Meng, S. P. Ong, *Sci. Rep.* **2016**, *6*, 33733.
- [24] W. D. Richards, T. Tsujimura, L. J. Miara, Y. Wang, J. C. Kim, S. P. Ong, I. Uechi, N. Suzuki, G. Ceder, *Nat. Commun.* **2016**, *7*, 11009.
- [25] H. Wang, Y. Chen, Z. D. Hood, G. Sahu, A. S. Pandian, J. K. Keum, K. An, C. Liang, *Angew. Chem., Int. Ed.* **2016**, *55*, 8551.
- [26] L. Zhang, D. Zhang, K. Yang, X. Yan, L. Wang, J. Mi, B. Xu, Y. Li, *Adv. Sci.* **2016**, *3*, 1600089.
- [27] D. H. Kim, D. Y. Oh, K. H. Park, Y. E. Choi, Y. J. Nam, H. A. Lee, S.-M. Lee, Y. S. Jung, *Nano Lett.* **2017**, *17*, 3013.
- [28] Y. E. Choi, K. H. Park, D. H. Kim, D. Y. Oh, H. R. Kwak, Y.-G. Lee, Y. S. Jung, *ChemSusChem* **2017**, *10*, 2605.
- [29] J. Jumas, F. Vermot-Gaud-Daniel, E. Philippot, *Cryst. Struct. Commun.* **1973**, *2*, 157.
- [30] J. Maier, *Nat. Mater.* **2005**, *4*, 805.
- [31] M. Avdeev, M. Sale, S. Adams, R. P. Rao, *Solid State Ionics* **2012**, *225*, 43.
- [32] X. He, Y. Zhu, Y. Mo, *Nat. Commun.* **2017**, *8*, 15893.
- [33] H. S. Ryu, J. S. Kim, J. S. Park, J. W. Park, K. W. Kim, J. H. Ahn, T. H. Nam, G. X. Wang, H. J. Ahn, *J. Electrochem. Soc.* **2013**, *160*, A338.